Overcoming the metamagnetic phase transition by epitaxial strain and its impact on magnetocaloric effect in Dy_2NiMnO_6 thin films

Saikarthikey Bhat [1], Wasim Akram [1], Manisha Bansal,[1] Aritra Dey [2], Bivas Saha [2] and Tuhin Maity [1,*]

[1] *School of Physics, Indian Institute of Science Education and Research Thiruvananthapuram, Thiruvananthapuram, Kerala 695551, India*

[2] *Chemistry and Physics of Materials Unit, Jawaharlal Nehru Centre for Advanced Scientific Research, Bangalore 560064, India*

(Received 21 May 2025; revised 12 September 2025; accepted 10 November 2025; published 10 December 2025)

Rare-earth-based double perovskites exhibit a large magnetocaloric effect, but often undergo first-order magnetic transitions because of the field-induced metamagnetic behavior. Since the first-order transitions involve a large hysteresis loss in a cooling cycle, suppression of the metamagnetic behavior is essential to improve the efficiency of such double perovskites. A promising approach for negating the loss of hysteresis involves modulating strain-sensitive magnetic interactions via thin films. In this work, we demonstrate that epitaxial strain significantly suppresses the metamagnetic behavior in epitaxial Dy_2NiMnO_6 grown on $SrTiO_3$ and $LaAlO_3$ compared to its bulk counterpart. Such epitaxial strain modifies the magnetic transition from the first order in bulk to the second order in thin films and significantly impacts the magnetocaloric properties. This difference is primarily attributed to strain-induced modifications in the Dy-(Ni/Mn) exchange interactions, driven by changes in the Ni-Mn exchange strength. Density functional theory calculations further confirm the role of strain in modifying the exchange interaction. Manipulating the order of magnetic phase transitions via strain engineering opens up the possibility of enhancing the magnetocaloric cooling efficiency in double perovskites and other first-order transition materials.

DOI: 10.1103/clty-4wr2

I. INTRODUCTION

Contemporary refrigeration technologies primarily rely on gas-compression-based cooling techniques that use chlorofluorocarbons and hydrochlorofluorocarbons, which are responsible for global warming and ozone layer depletion [1]. This obstructs the pursuit of a green and sustainable future. However, there exist sustainable alternatives such as thermoelectric cooling, thermoacoustic cooling, solid-state electrocaloric and magnetocaloric cooling, etc. [2]. Among these cooling techniques, magnetocaloric effect (MCE), i.e., cooling or heating of the material by withdrawing or applying a magnetic field, is most promising owing to the well-established parametrization techniques of the magnetic materials. Working prototypes of magnetocaloric refrigeration can achieve up to 60% of the ideal Carnot efficiency, compared to just 40% in the gas-compression-based system at its best [3]. However, certain challenges still remain, including the identification of suitable materials for an operation over a particular temperature range and the mitigation of the degrading efficiency over multiple cycles arising due to thermal hysteresis. These hinder the transition from laboratory to commercial scale.

To address such challenges, different material families are explored as magnetocaloric candidates, which include perovskite manganites [4,5], intermetallic alloys [6,7], spinel ferrites [8,9], etc. Among these, rare-earth-based perovskites (ABO_3, A^{3+} = rare-earth ions) are known to have a high magnitude of MCE, i.e., high entropy change ($-\Delta S_M$) values, along with better chemical stability and flexibility in modifying magnetocaloric properties [10–13]. In such perovskites, the transition metal (TM) ions, B^{3+}, interact through superexchange and double-exchange interactions mediated by oxygen. According to the Goodenough-Kanamori rules, these interactions are generally antiferromagnetic (AFM) in nature for a single oxidation state of the TM ions with a high transition temperature. Therefore, instead of one TM ion, if appropriate TM ion pairs, say, B and B', are introduced, the ferromagnetic (FM) or AFM interaction can selectively be tuned [14]. Such a family of compounds is referred to as double perovskites (DPs), with the general formula $A_2BB'O_6$, where A stands for rare-earth elements. These DPs have gained much attention for potential magnetocaloric cooling applications due to the presence of near-room-temperature magnetic transitions [15,16] and high magnetic entropy [17–19]. The A-site cation sometimes influences the magnetic interactions through $4f$-$3d$ and $4f$-$4f$ exchange interactions (at low temperatures), which gives rise to a high magnetic entropy change value at low temperature due to ordering of high-moment rare-earth (RE) ions [20,21]. This substantial change in magnetic entropy at low temperatures makes the DPs suitable for magnetic refrigeration below the hydrogen liquefaction temperature as well [22]. However, DPs often exhibit metamagnetic transitions due to strong $4f$-$3d$ interactions [23–25]. The system undergoing metamagnetic transitions is associated with first-order magnetic phase transitions (FOMPT), which lead to high thermal hysteresis and cyclic irreversibility [26–28]. Suppressing such a metamagnetic effect is therefore necessary to enhance the overall magnetocaloric efficiency. Tuning magnetic interactions in the material using external stimuli has been suggested as

*Contact author: tuhin@iisertvm.ac.in

a viable option [29–32]. The crystal structures of the DPs are mostly distorted owing to the balancing of the chemical pressure created by the different sizes of A- and B-site cations. The Goldschmidt tolerance factor, defined as $t = (r_A + r_O)/(\sqrt{2}(\langle r_B \rangle + r_O))$, where r_A, r_O, and r_B represent the radii of A, O, and average radii of the two B-site cations, respectively, is the measure of the $(B/B')O_6$ octahedral distortion [33]. Such an octahedral distortion alters the B-O-B' bond angles, which influence the exchange interactions. Strain engineering is a key method that can modify the bond angles and bond lengths, as well as induce octahedral distortions in the perovskite family [34,35]. This could lead to a modification in magnetic interactions. The epitaxially grown thin films can offer controlled strain through the choice of substrate, thickness, and defects to modulate the desired properties. This implies that the magnetic and magnetocaloric properties of a material can be tailored through the selection of an appropriate substrate, adjustment of thickness, and control of defects [36–38]. This makes the epitaxial thin films a promising technique to optimize the material's magnetocaloric properties. Among the DP thin films, the epitaxial A_2NiMnO_6 with $A =$ La and Nd are mostly studied with respect to strain, oxygen pressure, grain size, etc. [39–42]. Although the effect of strain on transition metal ions has been the primary focus of these reports, the rare-earth ion interactions under strain have been rarely explored. Therefore, investigating the rare-earth ions' interactions under epitaxial strain could be interesting as the order-disorder transition of the high-moment rare-earth ions involves a high entropy change at low temperature. Further, the influence of modified exchange interactions between the rare-earth and transition metal sites on magnetocaloric properties remains unexplored and warrants further investigation.

In this work, we report the suppression of the metamagnetic transition in Dy_2NiMnO_6 (DNMO) thin films epitaxially grown on $SrTiO_3$ (STO) and $LaAlO_3$ (LAO) substrates compared to the bulk counterpart, particularly in the temperature range of ∼20–50 K, where Dy-Ni/Mn($4f$-$3d$) interactions dominate [43,44]. This $4f$-$3d$ drives the field-induced metamagnetic transitions. As a result, the order of magnetic transition changes from first order to second order, potentially enabling work over multiple cooling cycles with minimal loss due to thermal hysteresis while sustaining the high magnetic entropy ($-\Delta S_M$). The two substrates impose different epitaxial strain states, and it is observed that higher strain results in stronger suppression of the metamagnetic transition together with enhanced cooling power. DC magnetization studies reveal that strain-induced modulation of Dy-(Ni/Mn) interactions in thin films is the reason for suppression of the metamagnetic nature. Further, the density functional theoretical (DFT) calculations reveal the role of epitaxial strain in modifying the strength of the exchange interaction. By suppressing the metamagnetic transition, rare-earth-based double perovskite thin films offer a promising path to improve magnetocaloric cooling efficiency in low-temperature refrigeration applications.

II. EXPERIMENT

Epitaxial thin films of DNMO were deposited on LAO and STO substrates using the pulsed laser deposition (PLD) technique by ablating the DNMO target (KrF excimer laser, with a wavelength of 248 nm). The deposition was carried out with a laser frequency of 5 Hz, laser energy density of $2 J/cm^2$, and a substrate temperature of 800 °C with oxygen pressure of 0.13 mbar. After deposition, *in situ* annealing was performed for 15 min at 800 °C under ambient oxygen pressure to ensure there were no oxygen vacancies in the film. The epitaxial growth was confirmed with the Rigaku x-ray diffractometer of Cu K_α (1.54 Å) in 2θ-ω geometry. The thickness of the film was measured by cross-section field emission scanning electron microscopy (FE-SEM). Magnetic measurements were carried out using a superconducting quantum interference device magnetometer (MPMS-3, Quantum Design) in the temperature (T) range of 2–300 K with a maximum magnetic field (H) of ±70 kOe. Before each magnetic measurement, the samples were demagnetized at 300 K, which is well above the transition temperature, using an appropriate demagnetization protocol [45].

DFT calculations were performed on DNMO bulk, as well as on strained DNMO grown on STO and LAO substrates. The changes in structural parameters, such as bond angles and bond lengths, induced by substrate strain, are investigated, and the influence of these structural modifications on the magnetic properties of the thin films compared to the bulk is studied. To avoid convergence issues commonly associated with $4f$ electrons, the $4f$ electrons of Dy were treated as core electrons and frozen in the calculations [46]. All density functional theory calculations were carried out using the projector augmented-wave (PAW) method with Perdew-Burke-Ernzerhof (PBE) pseudopotentials within the quantum espresso package. In order to incorporate correlations, Hubbard U was introduced by performing DFT + U calculations with suitable values of $U_{\text{eff}} = 5$ eV at the Mn and Ni sites [47]. A Monkhorst-Pack grid of $6 \times 6 \times 6$ k points was employed, with a kinetic energy cutoff of 50 Ry and a charge density cutoff of 400 Ry. These parameters, obtained from the self-consistent field calculations, were used for structural optimization and magnetic ground-state determination.

III. RESULTS AND DISCUSSION

A. Structural analysis

Figures 1(a) and 1(b) show the x-ray diffraction (XRD) (2θ-ω) of DNMO on STO and LAO, respectively. The pattern shows a single set of DNMO diffraction peaks together with those from the substrate, confirming the thin film's high purity. The existence of only ($00l$) reflections of substrate and film in thin films XRD confirms that the film grown on LAO and STO has a high degree of orientation along the c axis of the substrate. XRD shows c-axis strain of +1.5% and +0.5% for DNMO on STO and LAO, respectively. Thickness was found to be ∼30 nm for both DNMO grown on STO and LAO substrates, as determined by cross-sectional FE-SEM. The chosen thickness lies within the optimal range for probing strain, being thin enough to minimize relaxation while still thick enough to prevent the formation of a magnetic dead layer.

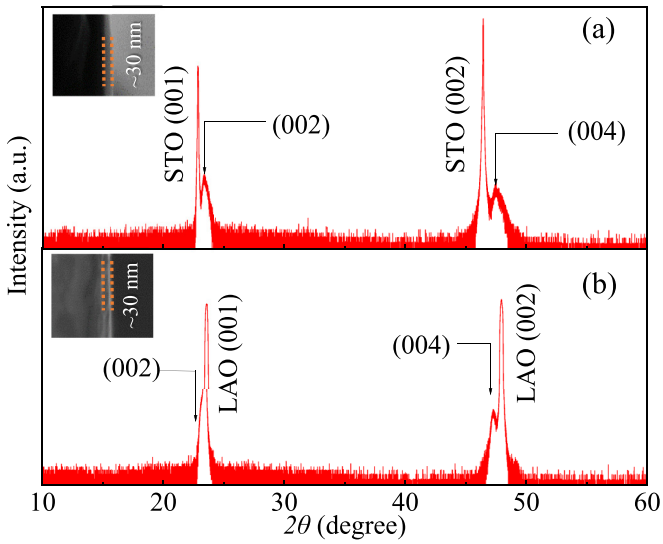

FIG. 1. (a) XRD scan (2θ-ω) of DNMO/STO. (b) XRD scan (2θ-ω) of DNMO/LAO. The inset shows cross-sectional FE-SEM images of DNMO/STO and DNMO/LAO.

B. Magnetic characterization

Temperature-dependent magnetization (MT curves) measured after zero-field cooling (ZFC) and field cooling (FC) for DNMO/STO, DNMO/LAO, and DNMO bulk [Figs. 2(a)–2(c)], respectively, under a $H \sim 0.1$ T. For ZFC, the sample was first cooled down to 2 K in the absence of any magnetic field. Then, field was applied, and the magnetization (M) was recorded while warming up. Subsequently, the FC-MT curve was recorded while cooling down again without removing H. For remanence magnetization measurement, H was set to zero, and then M was measured while warming up. The transition temperatures are identified using the extrema in the first derivative of magnetization, i.e., dM/dT vs T curves [insets of Figs. 2(a)–2(c)]. Figure 2(d) shows the remanence for all three samples. Both thin films (DNMO/STO and DNMO/LAO) exhibit two prominent peaks at 5 and 88 K in the dM/dT vs T curves. Similarly, in the bulk sample, two distinct peaks are observed, one at 5 K, but the other one at 92 K, as shown in the inset of Fig. 2(c). The low-temperature peak is attributed to Dy-Dy interactions for all three systems, while the high-temperature peaks arise due to Ni-Mn interactions in both the thin film and bulk samples [48]. However, the peak due to Ni-Mn interaction appears to be suppressed and shifted towards lower temperatures in thin films compared to bulk. The ZFC and FC-MT curves of thin films show a gradual increase with a decrement in temperature, which resembles the nature of AFM [49]. In contrast, ZFC and FC MT curves of bulk show a steep rise due to the ferromagnetic FM transition of Ni-Mn, in agreement with the previous report [43,50]. This indicates a change in the nature of Ni-Mn interaction in thin films compared to the bulk. Further, remanence data of thin films [Fig. 2(d)] show a sharp downturn below ∼50 K, whereas the remanence data of the bulk show a gradual increase. Below ∼50 K temperature, it has been reported that the rare-earth sublattice starts magnetically interacting with the TM sublattice [43,44,48,51]. In this temperature range, Ni-Mn interactions are well saturated, and Dy-Dy is too feeble to show any effect; thus, the prominent interaction in this temperature range (20–50 K) is Dy-Ni/Mn interactions. The sharp contrast in MT between thin films and bulk in the temperature range 20–50 K suggests modification in the magnetic interactions between Dy-(Ni/Mn) owing to the modification of Ni/Mn interactions.

Below ∼50 K, both DNMO/STO and DNMO/LAO show a remanence downturn due to Dy-Ni/Mn interactions [52,53]. However, at lower temperatures, a clear difference emerges between DNMO/STO and DNMO/LAO. In DNMO/STO, an upturn around ∼5 K appears, arising from stronger Dy-Dy interactions that compensate the Dy-Ni/Mn effect [inset Fig. 2(a)]. In contrast, DNMO/LAO exhibits no upturn, reflecting weaker Dy-Dy interactions, as also seen from the faint dM/dT peak near 5 K and reduced maximum entropy change compared to DNMO/STO [inset Figs. 2(b) and 4(e)]. To further understand the modification of Dy-Ni/Mn magnetic interactions in the range below 50 K, we study the behavior of coercivity (H_C) vs T.

Figures 3(a)–3(c) show magnetization vs magnetic field (MH) loops for all three samples over different T ranges, respectively. Figure 3(d) shows the variation of H_C with temperature for all three samples. H_C in the bulk sample was observed to increase monotonically as T decreases, which is in accordance with Stoner-Wohlfarth model. In contrast, the thin films (DNMO/STO and DNMO/LAO) exhibit a nonmonotonic behavior of H_C, showing a maximum near ∼40 K. The H_C behavior of the thin films deviates from this Stoner-Wohlfarth model, suggestive of a drastic modification in the magnetic interactions. This could be understood as

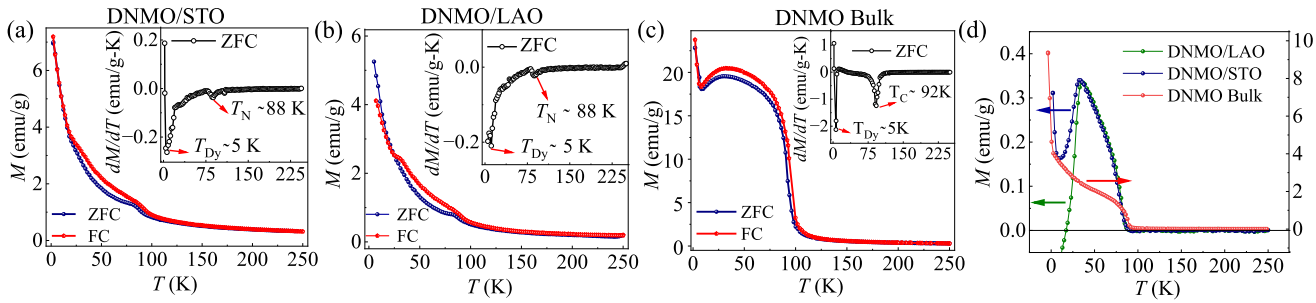

FIG. 2. MT curves of DNMO on STO at $H \sim 0.1$ T. (b) MT curve of DNMO on LAO at H ∼0.1 T. (c) MT curve of DNMO bulk at H ∼0.1 T. The inset shows dM/dT vs T curves extracted from ZFC MT. (d) Remanence of DNMO on LAO, DNMO on STO, and DNMO bulk.

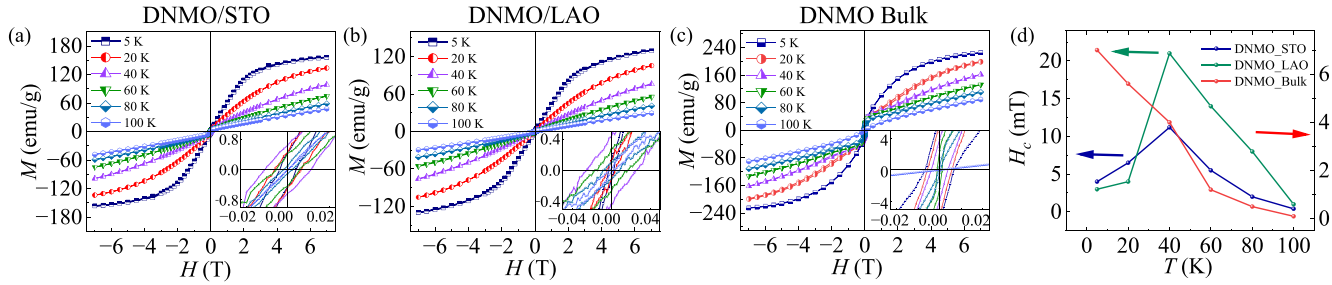

FIG. 3. (a)–(c) Isothermal MH loops for different temperatures for DNMO/STO, DNMO/LAO, and DNMO bulk. Insets show magnified low-field regions. (d) Temperature dependence of H_C for DNMO/STO, DNMO/LAO, and DNMO bulk.

follows: below the transition temperature of Ni–Mn (∼92 K for bulk and ∼88 K for thin films), H_C increases with decreasing temperature down to 40 K in both bulk and thin films, which is conventional. Below this temperature, Dy-Dy and Dy-(Ni/Mn) interactions become relevant, while the Ni-Mn exchange interactions are already saturated at higher temperatures. The Dy-Dy coupling is responsible for the long-range ordering of the Dy sublattice and is typically associated with very low coercivity [54,55]. However, the strength of Dy-Dy is much weaker than the Dy-Ni/Mn interaction in this regime, and therefore the softening of coercivity expected from Dy-Dy ordering cannot dominate the overall magnetic response [56]. Therefore, it could be inferred that the bulk DNMO exhibits stronger Dy-(Ni/Mn) interactions leading to monotonic behavior, but a observed decrease in H_C below 40 K in thin films suggests that Dy-(Ni/Mn) is not strong enough to mask the softening of coercivity due to Dy-Dy in thin films. This consolidates the weakening of Dy-(Ni/Mn) interaction in thin films. To confirm the change in strength of interaction, additional magnetic measurements were carried out.

Isothermal MH curves were measured from 5–115 K for all three samples [Figs. 4(a)–4(c)]. Isothermal MH curves of DNMO/STO and DNMO/LAO [Figs. 4(a) and 4(b)] show no special curvature related to metamagnetic, whereas the DNMO bulk [Fig. 4(c)] was found to display signs of metamagnetic transition in the temperature range ∼20–50 K. This coincides with the temperature range where Dy-(Ni/Mn) magnetic interactions are prominent; this observation is in agreement with our explanation of the weakening of Dy-(Ni/Mn) in thin films observed from MT and H_C vs T data. In bulk, Dy-(Ni/Mn) is said to have AFM interactions due to the negative $4f$-$3d$ interactions. This implies that there is an interplay of Zeeman and exchange energy in deciding the favorable magnetic alignment. In the low field, the exchange field between Dy and Ni/Mn dominates over the Zeeman field. However, once the applied field crosses a certain field, called a critical field, Zeeman energy takes over the exchange field. Now, the magnetic moment in the system will prefer to align along the direction of H [57]. This is observed as a change in the curvature in MH curves in bulk around ∼0–1 T. The absence of such behavior in the isothermal MH of thin films can be attributed to the fact that, even at low fields, the Dy spins align with the field direction with minimal resistance from the internal field (or exchange field) due to the net moment of Ni/Mn [58].

C. Magnetocaloric study

The impact of the change in magnetic interactions in RE-based DPs on MCE is studied elaborately. The magnetocaloric effect is quantified by the isothermal magnetic entropy change $-\Delta S_M(T, H)$ or by the adiabatic temperature change ΔT under a varying magnetic field. Disorder in magnetic spin is a measure of entropy. The application or removal of a magnetic field adiabatically decreases or increases the magnetic entropy. This change in magnetic entropy is compensated by a corresponding increase or decrease in lattice entropy, leading to a change in the system's temperature. Thus, magnetic entropy is directly related to the magnetocaloric effect (MCE). For thin films, calculating magnetic entropy from isothermal MH curves is preferred over direct measurement of adiabatic temperature change for experimental convenience [59]. The entropy changes $-\Delta S_M$ were calculated from the area between the consecutive isothermal MH curves (Fig. 4). The entropy change for variation of the magnetic field is given as follows [1,60]:

$$-\Delta S_M(T, H) = -\int_0^H \left(\frac{\partial M}{\partial T}\right)_H dH.$$

In practice, MH isotherms are taken at different temperatures with discrete temperature and magnetic field intervals. So, in order to calculate the $-\Delta S_M$ values, the above equation must be approximated to

$$-\Delta S_M = -\sum \frac{(M_n - M_{n+1})}{(T_n - T_{n+1})} \Delta H_n$$

Figures 4(d)–4(f) show the variation of $-\Delta S_M$ vs T plots for all three samples. In Figs. 4(d)–4(f), the arrows mark the $-\Delta S_M$ vs T curves corresponding to different magnetic field changes. The tail arrow denotes the curve for a field change from 0 to 2 T, while the head indicates the curve for a change from 0 to 5 T. Thus, the arrow direction illustrates the progression of $-\Delta S_M$ vs T curves with increasing magnetic field. DNMO/STO, DNMO/LAO, and DNMO bulk have the highest $-\Delta S_M$ of 13.76 (J/kg K), 10.386 (J/kg K), and 14.17 (J/kg K), respectively, under a 0–5 T change in the H. It is clear from the $-\Delta S_M$ vs T plots that all three samples show the highest entropy change around 5 K, due to Dy^{3+}–Dy^{3+} ordering. As reported in the literature, the largest entropy change in such systems typically occurs near the ordering temperature of the high-moment rare-earth sublattice. This is because $4f$-$4f$ exchange interactions, which drive rare-earth

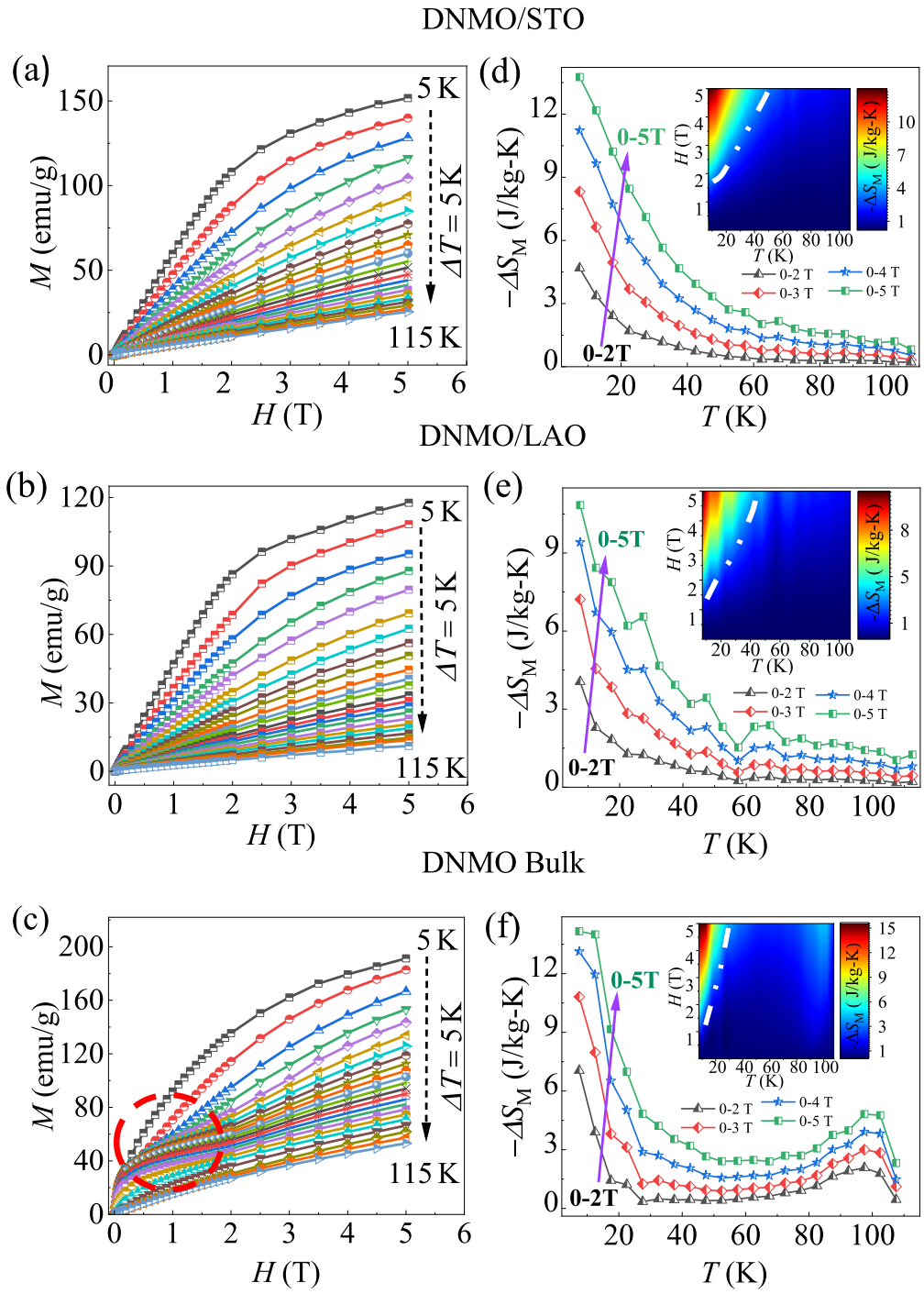

FIG. 4. (a)–(c) Isothermal MH curves for DNMO/STO, DNMO/LAO, and DNMO bulk, respectively. (d)–(f) $-\Delta S_M$ vs T for DNMO/STO, DNMO/LAO, and DNMO bulk, respectively. Insets show contour plots for all three samples.

ordering, are intrinsically weaker than both $4f$-$3d$ and $3d$-$3d$ interactions and therefore only become significant at low temperatures [20,43,61,62]. However, the comparably lower value of $-\Delta S_M$ in DNMO/LAO around 5 K is attributed to strain-induced weakening of Dy-Dy interactions, consistent with MT data. Thin films show no apparent peak in $-\Delta S_M$ around the ordering temperature of Ni^{2+}-Mn^{4+}, unlike bulk, where we see a clear peak around the Ni-Mn ordering temperature at ∼95 K. This is owing to the fact that FM interaction is weaker between Ni^{2+}-Mn^{4+} in thin films compared to bulk. Therefore, the change $-\Delta S_M$ around Ni^{2+}-Mn^{4+} is screened due to the high moment of Dy. Insets of Figs. 4(d)–4(f) show contour plot. This provides an intuitive visualization of the simultaneous evolution of $-\Delta S_M$ with temperature and field, which visually represents the effect of H and T on $-\Delta S_M$. This also clearly confirms the previous observation seen from $-\Delta S_M$ vs T plots.

Another important parameter for characterizing MCE is the relative cooling power (RCP). The RCP value signifies the amount of heat or energy a material can transfer in one cycle

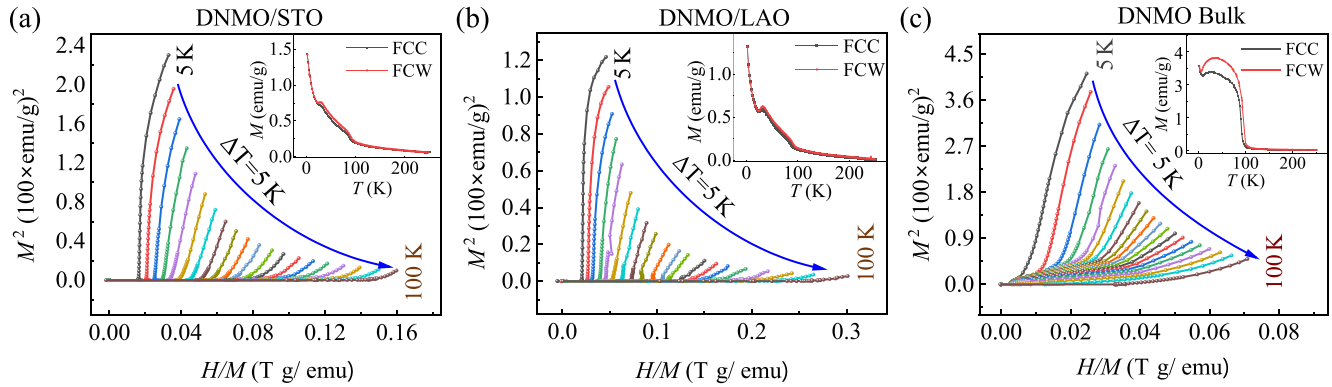

FIG. 5. (a)–(c) Arrott plot for DNMO/STO, DNMO/LAO and DNMO bulk, respectively. Insets show FCC-FCW at 0.02-T magnetic field.

from the surroundings to the heat sink. The value is calculated as follows [63,64]:

$$\mathrm{RCP} = \mathrm{Max}[-\Delta S_M(T,H)] \times \delta T_{\mathrm{FWHM}},$$

where $\mathrm{Max}(-\Delta S_M)$ is the maximum magnetic entropy change and δT_{FWHM} is the full width at half-maximum of the $-\Delta S_M(T)$ peak. RCP value of DNMO/STO, DNMO/LAO, and DNMO bulk is 287, 240, and 210 J/kg, respectively. The relatively higher RCP values in thin films compared to the bulk, despite the bulk exhibiting a higher $-\Delta S_M$, could be attributed to the broader low-temperature transition region in the thin films, which could be linked to modification of exchange interactions due to strain. The higher RCP value observed in thin films indicates that they can function over a wider temperature span while maintaining an appreciable magnetocaloric effect, thus, making thin film better suited for cryogenic applications. Furthermore, the higher RCP in DNMO/STO (+ 1.5% strain) relative to DNMO/LAO (+ 0.5% strain) directly indicates that the level of strain plays a crucial role in tuning the MCE properties. To further understand the nature of transition in thin films and bulk, we investigate the Arrott plot (M^2 vs H/M curves). Figures 5(a)–5(c) show the Arrott plot for DNMO thin films (DNMO/STO, DNMO/LAO) and bulk. By the Banerjee criterion, a positive slope means a second-order magnetic phase transition (SOMPT), while a negative slope points to a first-order transition [65]. The negative slope in the FOMPT appears because the magnetization jumps suddenly with field, showing that two magnetic states compete and the system releases latent heat. The thin films show a positive slope throughout the temperature range in the Arrott plot, indicating the second-order magnetic transition, whereas the bulk shows a negative slope, indicative of the first-order phase transition due to metamagnetic transition [66–68]. In a metamagnetic transition, the magnetization jump is triggered by the field, as the material switches from an AFM or weakly FM state to a FM state once the field crosses a certain threshold. Furthermore, field-cooled cooling (FCC) and field-cooled warming (FCW) MT curves [insets of Figs. 5(a)–5(c)] were also collected to confirm the order of transitions. Thus, the pronounced FCC-FCW bifurcation at low temperatures, where $4f$-$3d$ interactions are prominent, confirms the presence of FOMPT in the bulk due to metamagnetic transitions [27,67]. In contrast, the suppressed hysteresis and the positive slope in the Arrott plots for the thin films indicate a strain-driven suppression of metamagnetism, leading to a second-order magnetic phase transition (SOMPT). In the bulk samples [Fig. 5(c)], there is a large bifurcation between FCC and FCW in low temperatures, whereas in the thin films [Figs. 5(a) and 5(b)], this difference is very small. Such a large bifurcation is a hallmark of FOMPTs [69,70]. The hysteresis arises from latent heat and energy barriers between coexisting magnetic states, causing the system to follow different magnetization paths upon cooling and warming [71]. In a magnetic refrigeration cycle, this hysteresis represents irreversible processes; part of the input work is dissipated as heat rather than being reversibly converted into cooling power. As a result, thin-film samples can operate over multiple cycles with minimal energy loss. The weaker interactions between Dy-(Ni/Mn) are said to be the reason for the change in the order of magnetic transition from the first order to the second order transition [72,73].

The strain is considered to be responsible for such suppression in thin films due to modification of the exchange interactions.

D. DFT calculations

To study the effect of strain on magnetic ground states, we performed DFT calculations on bulk and strained states of DNMO. These optimized structures were used to calculate the magnetic ground states and the projected density of states (PDOS).

Table I displays the value of bond lengths, bond angles, and magnetic ground states for bulk DNMO and thin films. We observe that average Ni-O and Mn-O bonds are elongated 10%–12% and 2%–5%, respectively, in thin films compared to the bulk, and Ni-O-Mn deviates further away from the ideal 180° in thin films compared to the bulk. As shown

TABLE I. Ni-O and Mn-O bond lengths, Ni-O-Mn angles, and magnetic ground states (GS).

Material	Ni-O	Mn-O	Ni-O-Mn	GS
DNMO/STO	2.310 Å	2.063 Å	132.5°	AFM
DNMO/LAO	2.260 Å	2.009 Å	133.7°	AFM
DNMO bulk	2.060 Å	1.943 Å	144.9°	FM

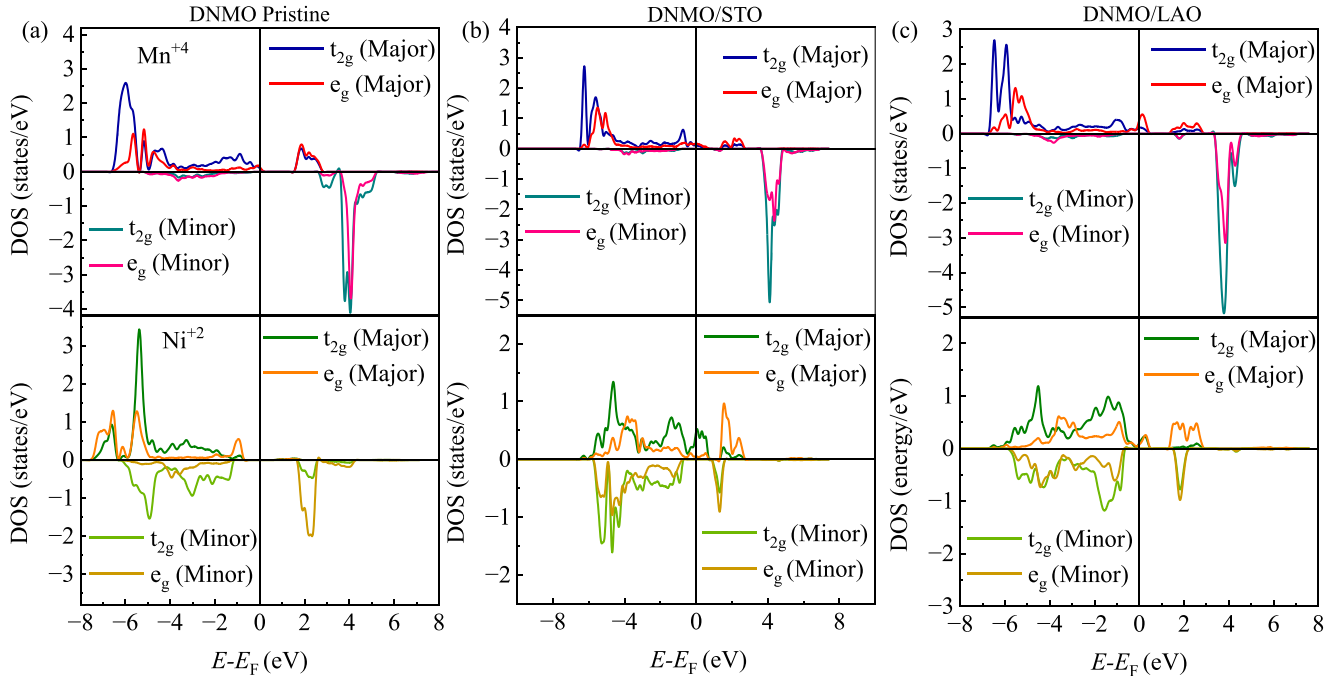

FIG. 6. (a)–(c) PDOS of d orbitals of Mn^{4+} (top) and Ni^{2+} (bottom) for DNMO/STO, and DNMO bulk, respectively.

from Table I, DNMO/STO exhibits a greater degree of distortion compared to DNMO/LAO, due to the higher strain induced by the substrate. This increased distortion can be correlated with the enhanced RCP value, which is attributed to strain-induced modifications in the exchange interactions. The magnetic ground state of the bulk was found to be FM, as the AFM configuration has a higher energy compared to the FM contribution. This FM ordering arises from the superexchange interactions due to electrons hopping from the half-filled e_g level of Ni^{2+} to the empty e_g level of Mn^{4+}, according to the Goodenough-Kanamori rules [74]. However, the magnetic ground state for thin films was found to be AFM, where the Mn^{4+} and Ni^{2+} moments align opposite to one another, irrespective of whether the initial configuration is AFM or FM [47]. Therefore, changes in bond lengths and bond angles in thin films due to strain lead to a change in exchange interactions [75,76].

Figures 6(a)–6(c) show the PDOS of Ni and Mn for all three samples. The transition metal ions Ni^{2+} (d^8) and Mn^{4+} (d^3) are coordinated by an oxygen octahedron, leading to the crystal-field-induced splitting of their d orbitals into t_{2g} (d_{xy}, d_{zx}, and d_{yz}) and e_g (d_{z^2} and $d_{x^2-y^2}$) levels. For DNMO bulk, both the majority-spin channel and the minority-spin channels of Ni-t_{2g} states are occupied, whereas only the majority-spin channel of Ni-e_g states is predominantly occupied. In contrast, the thin films, even the minority spin, are significantly occupied in Ni-e_g. This could be due to an increase in $\langle \mathrm{Ni-O} \rangle$, leading to a decrease in the crystal-field splitting. The effect of higher occupancy in the minority-spin channel in Ni-e_g, causes Ni-site to have a lower moment in thin films compared to DNMO bulk. However, for Mn, only the majority spin channel of Mn-t_{2g} is occupied, while the remaining states mostly remain unoccupied in both the bulk material and thin films. This is supported by the fact that the change in $\langle \mathrm{Ni-O} \rangle$ is comparatively higher than the change in $\langle \mathrm{Mn-O} \rangle$ for thin films compared to bulk. Therefore, the magnetic moment at the Mn site does not differ significantly between bulk and thin films. The strain-induced reduction of crystal-field splitting at the Ni site narrows the band gap, promoting metallic behavior in thin films compared to the insulating bulk [77,78].

The area under the DOS vs energy plots below the Fermi level (E_F) gives the value of occupancy of a particular state [79]. In bulk DNMO, occupancy of the majority-spin channel is higher than the minority-spin channel for both Ni and Mn. This indicates that the net moment of Ni and Mn align ferromagnetically. In thin films, occupancy in the majority spin is higher in Mn, and occupancy in the minority-spin channel is higher in Ni. Therefore, a net moment of Mn and Ni align opposite to one another, indicating AFM arrangement in thin films, in contrast to FM arrangement in bulk. Thus, DFT results further confirm that in thin films, AFM ordering of the Ni-Mn sublattice is energetically more favorable than the FM ordering observed in the bulk. This AFM preference reduces the net Ni-Mn moment, thereby lowering the exchange field exerted on the Dy sublattice [58]. This indicates that strain-induced modifications in Ni-Mn magnetic interaction in DNMO can be attributed to the suppression of metamagnetic transitions, which is in agreement with the experimental observations.

This suppression of the metamagnetic transitions in thin films can be understood using the AFM ground state calculated for Ni-Mn by DFT. In the regions below 50 K, the net exchange field due to Ni/Mn starts to interact with Dy spins via negative $4f$-$3d$ exchange interactions. However, the net moment of Ni/Mn in the thin films is much lower than in the bulk. Therefore, the alignment of Dy spins significantly alters the total magnetic moment in the thin films, whereas the bulk shows very minimal dependence. This can be observed by a gradual rise in ZFC and FC of thin films below Ni-Mn transition; in contrast, the MT curve of bulk remains flat in this

temperature range. This indicates that the net exchange field is weaker in the thin film compared to the bulk. The weaker exchange field suggests that Dy spins align along the magnetic field even in the low fields with minimal resistance from the internal field. Therefore, the metamagnetic transition, which is present in bulk due to competition between the exchange field ($4f$-$3d$ interaction) and the Zeeman field, is suppressed in thin films [80].

IV. CONCLUSION

In conclusion, the effect of strain on the order of transition and magnetocaloric effect is investigated in rare-earth-based double perovskite Dy_2NiMnO_6 thin films grown on STO and LAO using PLD. The XRD confirms high-quality c-axis-oriented epitaxial thin films of Dy_2NiMnO_6 grown on STO (001) and LAO (001). The metamagnetic transitions are found to be suppressed in thin films due to weakening of the Dy-(Ni/Mn) magnetic interactions because of the reduced exchange field of Ni/Mn under epitaxial strain. This reduction is further supported by our DFT calculations, which confirm the strain-induced weakening of Ni/Mn exchange field. As a consequence, a change in the order of magnetic transition from the first order as observed in bulk to second order in the thin films can be seen. Importantly, the change in order of transition does not cost any MCE value, which is advantageous for cooling applications. The induced second-order transition enables the thin films to operate over multiple cooling cycles with negligible energy loss due to thermal hysteresis compared to bulk at low-temperature ranges. This opens a new avenue for increasing the magnetocaloric efficiency of high-moment rare-earth-based double perovskites.

ACKNOWLEDGMENTS

S.B. and T.M. acknowledge institute funding from IISER Thiruvananthapuram, Center for High-Performance Computing (CHPC), IISER Thiruvananthapuram for access to the cluster. S.B. and T.M. acknowledge the helium Plant funded by DST for providing the liquid helium for magnetic measurement with SQUID. W.A. and T.M. acknowledge financial support from DST Inspire. M.B. acknowledges support from a Prime Minister Research Fellowship (PMRF) and institute funding from IISER Thiruvananthapuram.

DATA AVAILABILITY

The data that support the findings of this article are not publicly available upon publication because it is not technically feasible and/or the cost of preparing, depositing, and hosting the data would be prohibitive within the terms of this research project. The data are available from the authors upon reasonable request.

[1] M.-H. Phan and S.-C. Yu, Review of the magnetocaloric effect in manganite materials, J. Magn. Magn. Mater. **308**, 325 (2007).

[2] A. Kitanovski, Energy applications of magnetocaloric materials, Adv. Energy Mater. **10**, 1903741 (2020).

[3] V. Franco, J. Blázquez, B. Ingale, and A. Conde, The magnetocaloric effect and magnetic refrigeration near room temperature: Materials and models, Annu. Rev. Mater. Res. **42**, 305 (2012).

[4] Z. B. Guo, Y. W. Du, J. S. Zhu, H. Huang, W. P. Ding, and D. Feng, Large magnetic entropy change in perovskite-type manganese oxides, Phys. Rev. Lett. **78**, 1142 (1997).

[5] M. Phan, V. Pham, S. Yu, J. Rhee, and N. Hur, Large magnetic entropy change in a $La_{0.8}Ca_{0.2}MnO_3$ single crystal, J. Magn. Magn. Mater. **272-276**, 2337 (2004).

[6] A. O. Pecharsky, K. Gschneidner, Jr., V. Pecharsky, and C. Schindler, The room temperature metastable/stable phase relationships in the pseudo-binary Gd_5Si_4–Gd_5Ge_4 system, J. Alloys Compd. **338**, 126 (2002).

[7] H. Wada and Y. Tanabe, Giant magnetocaloric effect of $MnAs_{1-x}Sb_x$, Appl. Phys. Lett. **79**, 3302 (2001).

[8] S. Bahhar, A. Boutahar, L. Omari, H. Lemziouka, E. Hlil, H. Bioud, and E. Dhahri, Structural, magnetic and magnetocaloric properties of $TMCeFeO_4$ (TM = Mn, Co) spinel ferrites powders, J. Magn. Magn. Mater. **539**, 168416 (2021).

[9] H. Qin, Y. He, P. Xu, D. Huang, Z. Wang, H. Wang, Z. Wang, Y. Zhao, Q. Tian, and C. Wang, Spinel ferrites (MFe_2O_4): Synthesis, improvement and catalytic application in environment and energy field, Adv. Colloid Interface Sci. **294**, 102486 (2021).

[10] A. O. Ayaş, S. K. Çetin, M. Akyol, G. Akça, and A. Ekicibil, Effect of b site partial ru substitution on structural magnetic and magnetocaloric properties in $La_{0.7}Pb_{0.3}Mn_{1-x}RuxO_3$ (X = 0.0, 0.1 and 0.2) perovskite system, J. Mol. Struct. **1200**, 127120 (2020).

[11] W. Zhong, C.-T. Au, and Y.-W. Du, Review of magnetocaloric effect in perovskite-type oxides, Chin. Phys. B **22**, 057501 (2013).

[12] M. Balli, P. Fournier, S. Jandl, and M. Gospodinov, A study of the phase transition and magnetocaloric effect in multiferroic La_2MnNiO_6 single crystals, J. Appl. Phys. **115**, 173904 (2014).

[13] T. M. Al-Shahumi, I. A. Al-Omari, S. H. Al-Harthi, and M. T. Z. Myint, Synthesis, structure, morphology, magnetism, and magnetocaloric-effect studies of $(La_{1-x}PrX)_{0.7}Sr_{0.3}MnO_3$ nanocrystalline perovskites, SN Appl. Sci. **5**, 121 (2023).

[14] C. Bull, D. Gleeson, and K. Knight, Determination of b-site ordering and structural transformationsin the mixed transition metal perovskites La_2CoMnO_6 and La_2NiMnO_6, J. Phys.: Condens. Matter **15**, 4927 (2003).

[15] M. Nasir, M. Khan, S. Kumar, S. Bhatt, N. Patra, D. Bhattacharya, S. N. Jha, S. Biring, and S. Sen, The effect of high temperature annealing on the antisite defects in ferromagnetic La_2NiMnO_6 double perovskite, J. Magn. Magn. Mater. **483**, 114 (2019).

[16] R. Sharma, N. Hooda, A. Hooda, and S. Khasa, Structural, dielectric and magnetic study of double perovskite La_2CoMnO_6, Phys. B (Amsterdam) **673**, 415473 (2024).

[17] J. Moon, M. Kim, Y. J. Choi, and N. Lee, Giant anisotropic magnetocaloric effect in double-perovskite Gd_2CoMnO_6 single crystals, Sci. Rep. **7**, 16099 (2017).

[18] Y. Zhang, Y. Tian, Z. Zhang, Y. Jia, B. Zhang, M. Jiang, J. Wang, and Z. Ren, Magnetic properties and giant cryogenic magnetocaloric effect in B-site ordered antiferromagnetic Gd_2MgTiO_6 double perovskite oxide, Acta Mater. **226**, 117669 (2022).

[19] J. K. Murthy, K. D. Chandrasekhar, S. Mahana, D. Topwal, and A. Venimadhav, Giant magnetocaloric effect in Gd_2NiMnO_6 and Gd_2CoMnO_6 ferromagnetic insulators, J. Phys. D: Appl. Phys. **48**, 355001 (2015).

[20] Y. Zhang, Y. Na, W. Hao, T. Gottschall, and L. Li, Enhanced cryogenic magnetocaloric effect from 4f-3d exchange interaction in B-site ordered Gd_2CuTiO_6 double perovskite oxide, Adv. Funct. Mater. **34**, 2409061 (2024).

[21] S. Zheng, C. Li, C. Bai, K. Zhou, P. Wang, Y. Lu, Y. Qiu, and Y. Luo, Magnetic properties and enhanced cryogenic magnetocaloric effect in ti-substituted Gd_2CoMnO_6 double perovskites, J. Magn. Magn. Mater. **564**, 170162 (2022).

[22] T. Numazawa, K. Kamiya, T. Utaki, and K. Matsumoto, Magnetic refrigerator for hydrogen liquefaction, Cryogenics **62**, 185 (2014).

[23] M. Kim, J. Moon, S. Oh, D. Oh, Y. Choi, and N. Lee, Strong magnetoelectric coupling in mixed ferrimagnetic-multiferroic phases of a double perovskite, Sci. Rep. **9**, 5456 (2019).

[24] M.-R. Li, P. W. Stephens, M. Croft, Z. Deng, W. Li, C. Jin, M. Retuerto, J. P. Hodges, C. E. Frank, M. Wu *et al.*, $Mn_2(Fe_{0.8}Mo_{0.2})MoO_6$: A double perovskite with multiple transition metal sublattice magnetic effects, Chem. Mater. **30**, 4508 (2018).

[25] A. Harbi, Y. Legodec, H. Moutaabbid, S. Benmokhtar, and M. Moutaabbid, Tailoring the Griffiths-like cluster formation in the insulator ferromagnet spin-glass $Gd_2Ni_xCo_{1-x}MnO_6$ double perovskite, Phys. Rev. B **104**, 054404 (2021).

[26] M. Şaşmaz, Metamagnetic transition and magnetocaloric properties of $Ni_{45}Mn_{42}In_{13}$ Heusler alloy, Phase Transitions **94**, 289 (2021).

[27] G. Kotnana, P. D. Babu, and S. Jammalamadaka, Metamagnetic transitions and magnetocaloric properties of $HoCr_{1-x}Fe_xO_3$ (x = 0.25 and 0.75) compounds, J. Supercond. Novel Magn. **35**, 2057 (2022).

[28] W.-L. Zuo, A. Murtaza, A. Ghani, Y. Ding, L. Liu, and S. Yang, Metamagnetic phase transition and corresponding magnetocaloric effect in intermetallic $Ho_{1-x}Tb_xCo_2$ alloys, J. Alloys Compd. **1002**, 175216 (2024).

[29] X. Moya, L. Hueso, F. Maccherozzi, A. Tovstolytkin, D. Podyalovskii, C. Ducati, L. Phillips, M. Ghidini, O. Hovorka, A. Berger *et al.*, Giant and reversible extrinsic magnetocaloric effects in $La_{0.7}Ca_{0.3}MnO_3$ films due to strain, Nat. Mater. **12**, 52 (2013).

[30] Y. Liu, T. Ma, K. Qiao, J. Li, A. Xiao, J. Wang, F. Hu, and B. Shen, Strain control of phase transition and magnetocaloric effect in $Nd_{0.5}Sr_{0.5}MnO_3$ thin films, Appl. Phys. Lett. **116**, 082402 (2020).

[31] B. Dabrowski, J. Mais, S. Kolesnik, and O. Chmaissem, Parameters controlling magnetic interactions in perovskite manganites, J. Phys.: Conf. Ser. **303**, 012057 (2011).

[32] J. M. De Teresa, M. R. Ibarra, J. Blasco, J. Garcia, C. Marquina, P. A. Algarabel, Z. Arnold, K. Kamenev, C. Ritter, and R. Von Helmolt, Spontaneous behavior and magnetic field and pressure effects on $La_{2/3}Ca_{1/3}MnO_3$ perovskite, Phys. Rev. B **54**, 1187 (1996).

[33] H. Liu and X. Yang, A brief review on perovskite multiferroics, Ferroelectrics **507**, 69 (2017).

[34] A. Arulraj, R. E. Dinnebier, S. Carlson, M. Hanfland, and S. van Smaalen, Strain effects in perovskite manganites, Prog. Solid State Chem. **35**, 367 (2007).

[35] D. Sando, Strain and orientation engineering in ABO_3 perovskite oxide thin films, J. Phys.: Condens. Matter **34**, 153001 (2022).

[36] Y. Sakurai, I. Ohkubo, Y. Matsumoto, H. Koinuma, and M. Oshima, Influence of substrates on epitaxial growth of B-site-ordered perovskite La_2NiMnO_6 thin films, J. Appl. Phys. **110**, 063913 (2011).

[37] S. K. Giri, W. Akram, M. Bansal, and T. Maity, Tuning the magnetocaloric effect by optimizing thickness-induced three-dimensional strain states, Phys. Rev. B **104**, 224432 (2021).

[38] W. Akram, Y. Saha, S. Bhat, and T. Maity, Impact of antiphase boundary on the magnetocaloric effect in geometrically frustrated epitaxial $MnCr_2O_4$, Appl. Phys. Lett. **126**, 222404 (2025).

[39] D. Matte, M. de Lafontaine, A. Ouellet, M. Balli, and P. Fournier, Tailoring the magnetocaloric effect in La_2NiMnO_6 thin films, Phys. Rev. Appl. **9**, 054042 (2018).

[40] A. K. Singh, S. Chauhan, P. Balasubramanian, S. K. Srivastava, and R. Chandra, Influence of substrate induced strain on B-site ordering and magnetic properties of Nd_2NiMnO_6 epitaxial thin films, Thin Solid Films **629**, 49 (2017).

[41] J. P. Palakkal, T. Schneider, and L. Alff, Oxygen defect engineered magnetism of La_2NiMnO_6 thin films, AIP Adv. **12**, 035116 (2022).

[42] D. Kumar and D. Kaur, Structural and magnetic properties of La_2NiMnO_6 thin films on $LaAlO_3$ substrate with varying thickness, J. Alloys Compd. **554**, 277 (2013).

[43] M. Balli, S. Mansouri, P. Fournier, S. Jandl, K. Truong, S. K.-H. Khlifa, P. de Rango, D. Fruchart, and A. Kedous-Lebouc, Enlarging the magnetocaloric operating window of the Dy_2NiMnO_6 double perovskite by lanthanum doping, J. Phys. D: Appl. Phys. **53**, 095001 (2020).

[44] J. K. Murthy and A. Venimadhav, 4f-3d exchange coupling induced exchange bias and field induced Hopkinson peak effects in Gd_2CoMnO_6, J. Alloys Compd. **719**, 341 (2017).

[45] T. Maity, S. Goswami, D. Bhattacharya, and S. Roy, Superspin glass mediated giant spontaneous exchange bias in a nanocomposite of $BiFeO_3$-$Bi_2Fe_4O_9$, Phys. Rev. Lett. **110**, 107201 (2013).

[46] H. J. Zhao, W. Ren, X. M. Chen, and L. Bellaiche, Effect of chemical pressure, misfit strain and hydrostatic pressure on structural and magnetic behaviors of rare-earth orthochromates, J. Phys.: Condens. Matter **25**, 385604 (2013).

[47] A. Ghosh, R. Roy, R. C. Sahoo, S. N. Sarangi, M. Ghosh, D. Mazumdar, D. Samal, P. S. A. Kumar, Z. Hossain, S. Kanungo *et al.*, Magnetic anisotropy and magnetocaloric effect in Gd_2NiMnO_6 thin films, Phys. Rev. B **108**, 214423 (2023).

[48] Y. Jia, Q. Wang, Y. Qi, and L. Li, Multiple magnetic phase transitions and magnetocaloric effect in double perovskites R_2NiMnO_6 (R = Dy, Ho, and Er), J. Alloys Compd. **726**, 1132 (2017).

[49] R. Das, A. Jaiswal, and P. Poddar, Static and dynamic magnetic properties and interplay of Dy^{3+}, Gd^{3+} and Mn^{3+} spins in orthorhombic $DyMnO_3$ and $GdMnO_3$ nanoparticles, J. Phys. D: Appl. Phys. **46**, 045301 (2013).

[50] M. G. Masud, K. Dey, A. Ghosh, S. Majumdar, and S. Giri, Occurrence of magnetoelectric effect correlated to the Dy order in Dy_2NiMnO_6 double perovskite, J. Appl. Phys. **118**, 064104 (2015).

[51] Y. Xin, L. Shi, J. Zhao, X. Yuan, S. Zhou, L. Hou, and L. Yang, Nature of Griffiths phase and ferromagnetic 3d-4f interaction in double-perovskite Dy_2CoMnO_6, J. Alloys Compd. **893**, 162222 (2022).

[52] O. Peña, M. Guilloux-Viry, A. Antunes, W. Peng, Y. Ma, Z. Gao, and C. Moure, Magnetization reversal in bulk and thin films of the ferrimagnetic $ErCo_{0.50}Mn_{0.50}O_3$ perovskite, J. Magn. Magn. Mater. **321**, 1723 (2009).

[53] K. Aswathi, J. P. Palakkal, R. Revathy, and M. R. Varma, Sign reversal of magnetization in Sm_2CrMnO_6 perovskites, J. Magn. Magn. Mater. **483**, 89 (2019).

[54] J. Shi, S. Yin, M. S. Seehra, and M. Jain, Enhancement in magnetocaloric properties of $ErCrO_3$ via a-site Gd substitution, J. Appl. Phys. **123**, 193901 (2018).

[55] J. Shi, T. Sauyet, Y. Dang, S. L. Suib, M. S. Seehra, and M. Jain, Structure-property correlations and scaling in the magnetic and magnetocaloric properties of $GdCrO_3$ particles, J. Phys.: Condens. Matter **33**, 205801 (2021).

[56] A. McDannald, L. Kuna, and M. Jain, Magnetic and magnetocaloric properties of bulk dysprosium chromite, J. Appl. Phys. **114**, 113904 (2013).

[57] A. Banerjee, J. Sannigrahi, S. Giri, and S. Majumdar, Magnetization reversal and inverse exchange bias phenomenon in the ferrimagnetic polycrystalline compound Er_2CoMno_6, Phys. Rev. B **98**, 104414 (2018).

[58] W. Akram, M. Bansal, R. P. Pradeep, A. Kaipamangalath, S. K. Giri, and T. Maity, Evolution of the inverse magnetocaloric effect for random-field to spin-glass crossover in Sm Ca Co Mn O_6-Sm Mn O_3 nanocomposite, Phys. Rev. B **107**, 224403 (2023).

[59] J. H. Belo, A. L. Pires, J. P. Araujo, and A. M. Pereira, Magnetocaloric materials: From micro-to nanoscale, J. Mater. Res. **34**, 134 (2019).

[60] N. A. de Oliveira and P. J. von Ranke, Theoretical aspects of the magnetocaloric effect, Phys. Rep. **489**, 89 (2010).

[61] Z. Yang, J.-Y. Ge, S. Ruan, H. Cui, and Y.-J. Zeng, Cryogenic magnetocaloric effect in distorted double-perovskite Gd_2ZnTiO_6, J. Mater. Chem. C **9**, 6754 (2021).

[62] Meenakshi, S. Saini, N. Panwar, Ramovatar, and S. Kumar, Giant magnetocaloric properties of Gd-based double perovskite compounds in cryogenic temperature range, J. Magn. Magn. Mater. **614**, 172766 (2025).

[63] M. Wood and W. Potter, General analysis of magnetic refrigeration and its optimization using a new concept: Maximization of refrigerant capacity, Cryogenics **25**, 667 (1985).

[64] S. Chatterjee and I. Das, Magnetic properties and universal behavior of magnetocaloric effect for polycrystalline $(Nd_{0.5}Sm_{0.5})_{0.5}Sr_{0.5}MnO_3$ compound, J. Alloys Compd. **935**, 167957 (2023).

[65] V. S. Kolat, T. Izgi, A. O. Kaya, N. Bayri, H. Gencer, and S. Atalay, Metamagnetic transition and magnetocaloric effect in charge-ordered $Pr_{0.68}Ca_{0.32-x}Sr_xMnO_3$ (x=0, 0.1, 0.18, 0.26 and 0.32) compounds, J. Magn. Magn. Mater. **322**, 427 (2010).

[66] B. Banerjee, On a generalised approach to first and second order magnetic transitions, Phys. Lett. **12**, 16 (1964).

[67] C. Li, L. Wang, X. Li, C. Zhu, R. Zhang, H. Wang, and S. Yuan, Magnetic field-induced metamagnetism and magnetocaloric effect in double perovskites Re_2CoMnO_6 (Re= Sm, Dy), Mater. Chem. Phys. **202**, 76 (2017).

[68] S. Bustingorry, F. Pomiro, G. Aurelio, and J. Curiale, Second-order magnetic critical points at finite magnetic fields: Revisiting arrott plots, Phys. Rev. B **93**, 224429 (2016).

[69] B. Dalal, B. Sarkar, V. D. Ashok, and S. K. De, Magnetization reversal, exchange interaction, and switching behavior studies on Ru doped $GdCrO_3$, J. Alloys Compd. **739**, 418 (2018).

[70] K. Xu, Z. Li, E. Liu, H. Zhou, Y. Zhang, and C. Jing, Magnetocaloric effect and negative thermal expansion in hexagonal Fe doped MnNiGe compounds with a magnetoelastic AFM-FM-like transition, Sci. Rep. **7**, 41675 (2017).

[71] T. Poudel Chhetri, J.-H. Chen, A. T. Grant, D. P. Young, I. Dubenko, S. Talapatra, N. Ali, and S. Stadler, Effects of doping, hydrostatic pressure, and thermal quenching on the phase transitions and magnetocaloric properties in $Mn_{1-x}Co_xNiGe$, J. Appl. Phys. **132**, 045107 (2022).

[72] K. Anand, A. Pal, M. Alam, S. Dan, S. Kumar, S. Ghosh, S. Kumari, A. Das, M. Sawada, A. Mohan *et al.*, Emergence of metamagnetic transition, re-entrant cluster glass and spin phonon coupling in Tb_2CoMnO_6, J. Phys.: Condens. Matter **33**, 275802 (2021).

[73] M. Kim, J. Moon, H. Choi, S. Oh, N. Lee, and Y. Choi, Investigation of the magnetic properties in double perovskite R_2CoMnO_6 single crystals (R= rare earth: La to lu), J. Phys.: Condens. Matter **27**, 426002 (2015).

[74] J. B. Goodenough, Goodenough-Kanamori rule, Scholarpedia **3**, 7382 (2008).

[75] M. Nasir, S. Kumar, N. Patra, D. Bhattacharya, S. N. Jha, D. R. Basaula, S. Bhatt, M. Khan, S.-W. Liu, S. Biring *et al.*, Role of antisite disorder, rare-earth size, and superexchange angle on band gap, curie temperature, and magnetization of R_2NiMnO_6 double perovskites, ACS Appl. Electron. Mater. **1**, 141 (2019).

[76] E.-M. Choi, T. Maity, A. Kursumovic, P. Lu, Z. Bi, S. Yu, Y. Park, B. Zhu, R. Wu, V. Gopalan *et al.*, Nanoengineering room temperature ferroelectricity into orthorhombic $SmMnO_3$ films, Nat. Commun. **11**, 2207 (2020).

[77] A. Paul and U. V. Waghmare, First-principles prediction of a polar half-metallic ferromagnet in a heterostructure based on $PbMnO_3$ and $SrMnO_3$, Phys. Rev. B **110**, 184110 (2024).

[78] P.-H. Xiang, N. Zhong, C.-G. Duan, X. Tang, Z. Hu, P. Yang, Z. Zhu, and J. Chu, Strain controlled metal-insulator transition in epitaxial $NdNiO_3$ thin films, J. Appl. Phys. **114**, 243713 (2013).

[79] W. Kohn and L. J. Sham, Self-consistent equations including exchange and correlation effects, Phys. Rev. **140**, A1133 (1965).

[80] Y. Long, Q. Liu, Y. Lv, R. Yu, and C. Jin, Various 3*d*-4*f* spin interactions and field-induced metamagnetism in the Cr^{5+} system $DyCrO_4$, Phys. Rev. B **83**, 024416 (2011).